Contribution to the analysis of the predissociated rovibronic structure of the symmetric isotopomers 16O3 and 18O3 of ozone near 10,400 cm-1: 3A2(A20)

Wannous, Ghassan; Bouvier, A. J.; El Helou, Z.; Chillier, Xavier; Churassy, S.; Bacis, R.; Campargue, Alain; Weirauch, G.; Judge, R. H.

Available online at www.sciencedirect.com
SCIENCE DIRECT®
Spectrochimica Acta Part A 60 (2004) 889–898
SPECTROCHIMICA ACTA PART A
www.elsevier.com/locate/saa

Contribution to the analysis of the predissociated rovibronic structure of the symmetric isotopomers $^{16}O_3$ and $^{18}O_3$ of ozone near 10,400 cm^{-1}: $^3A_2(3_0^2) \leftarrow \tilde{X}^1A_1(0_0^0)$ and $^3B_2 \leftarrow \tilde{X}^1A_1$

G. Wannous [a,*], A.J. Bouvier [a], Z. El Helou [a], X. Chillier [a], S. Churassy [a], R. Bacis [a], A. Campargue [b], G. Weirauch [b], R.H. Judge [c]

[a] *Laboratoire de Spectrométrie Ionique et Moléculaire, UMR CNRS No. 5579, Université Claude Bernard Lyon 1, 43 Boulevard du 11 Novembre 1918, 69622 Villeurbanne Cedex, France*
[b] *Laboratoire de Spectrométrie Physique, Université Joseph Fourier de Grenoble, BP 87, 38402 Saint Martin d'Hères Cedex, France*
[c] *Department of Chemistry, University of Wisconsin-Parkside, Kenosha, WI 53141-2000, USA*

Received 7 March 2003; accepted 9 July 2003

Abstract

The absorption spectrum of ozone was recorded at low temperatures (down to −135 °C) by high resolution Fourier transform spectrometry and intra cavity laser absorption spectroscopy (ICLAS) near 10,400 cm^{-1}. A preliminary analysis of the rotational structure of the absorption spectra of $^{16}O_3$ and $^{18}O_3$ shows that this spectral region corresponds to a superposition of two different electronic transitions, one with a very broad rotational structure, showing for the first time the asymmetric stretching frequency mode ν_3 of the electronic state $^3A_2$, the other formed by a completely diffuse band, probably the 2_0^1 band of a new transition due to the triplet electronic state $^3B_2$. Predissociation effects induce large broadening of the rotational lines for the transition centered at 10,473 cm^{-1} identified as the 3_0^2 band of the $^3A_2 \leftarrow \tilde{X}^1A_1$ electronic transition. The rotational structure cannot be analyzed directly but instead the band contour method was used to confirm the symmetry of the transition and to estimate the spectroscopic constants for the ^{16}O isotopomer. The origin of the band is at 10,473 ± 3 cm^{-1} and the value of the $^{16}O_3(^3A_2)$ antisymmetric stretching frequency mode is equal to 460 ± 2 cm^{-1}. We believe that the diffuse band is due to the $^3B_2$ state and is located at about 10,363 ± 3 cm^{-1} for $^{16}O_3$ and 10,354 ± 3 cm^{-1} for $^{18}O_3$. The isotopic rules confirm the different results obtained for $^{18}O_3$ and $^{16}O_3$.

Keywords: Ozone; $^{16}O_3$; $^{18}O_3$; Electronic spectroscopy; Wulf transition; Intra cavity laser absorption spectroscopy (ICLAS)

1. Introduction

Absorption of solar radiation by the ozone molecule plays a major role in the atmosphere through important chemical transformations in the troposphere, stratosphere and mesosphere. As a consequence, extensive theoretical [1–7] and experimental efforts [8–13] have been undertaken to determine the structure, spectroscopy and excited states of ozone during this last decade.

The five lowest-lying excited electronic states of ozone contribute to the absorption in the near infrared up to visible region (Wulf and Chappuis bands). For one of these states, we have successfully completed a mixed line-by-line and band contour analysis of the 0_0^0 band [10c,14a] of the $^3A_2 \leftarrow \tilde{X}^1A_1$ transition. We have also been able to determine the lifetime of the $^3A_2$ state [10c,15]. These results demonstrate the bound and metastable character of this state but show that the lifetime is drastically reduced by predissociation processes which eliminate the hypothetical role of "hidden" ozone in the related excited state for the observed range of high K and high J values.

In a review about ozone [16], we suggested that the absorption spectra recorded by Fourier transform spectrometry, in the region 10,460 cm^{-1}, involve the $^3B_2 \leftarrow \tilde{X}^1A_1$ transition with $T_0 = 10{,}458 \pm 5$ cm^{-1} (1.2966±0.0006 eV).[1] The

* Corresponding author. Tel.: +33-4-72-44-85-58; fax: +33-4-72-44-58-71.
E-mail address: wannous@lasim.univ-lyon1.fr (G. Wannous).

[1] A manuscript error has been introduced in the paper of [16], page 20 last line and Table 3 (caption b) maximum peak at 10,456 ± 1 cm^{-1}

1386-1425/$ – see front matter © 2003 Elsevier B.V. All rights reserved.
doi:10.1016/S1386-1425(03)00316-0

Table 1

State	Theory			Experiment	
	T_e (T_0)[a] [2]	T_0 [1a][a]	T_e [5]	T_0 [11]	T_0 [8][a] (eV)
$^3A_2$	0.90 (0.92)	1.15	0.86	1.18	1.184 ± 0.002
$^3B_2$	1.19 (1.18)	1.33	1.10	1.30	1.29 ± 0.03
$^3B_1$	1.18 (1.16)	1.33	1.27	1.45	1.45 ± 0.03
$^1A_2$	1.15 (1.14)	1.44	1.44	≅1.6	
$^1B_1$	1.65 (1.64)	1.88	1.82		1.98

T_0 (or T_e) of the five lowest excited states of the ozone molecule were calculated using multi-configurational second-order perturbation theory (CASPT2) [1a]. The calculation was carried out for the ground and seven low-lying singlet and triplet excited states of ozone and the ground state of ozonide anion in C_{2v} symmetry by the complete active space self-consistent field (CASSCF) and the multi-reference Meller–Plesset perturbation (MRMP) [2]. Calculated adiabatic energies relative to $\tilde{X}^1A_1$ under C_{2v} symmetry as obtained from MRD-CI potential energy surfaces ($\tilde{X}^1A_1$ and the first 12 states of the ozone molecule) [5]. From absorption spectroscopy [8]. Anion photoelectron spectroscopy [11].

[a] Only the symmetric vibrational modes used for the calculation of the ZPE corrections.

$^3B_2$ state shares the same dissociation limit [$O_2(^3\Sigma_g^-, v = 0) + O(^3P)$] as the ground state $\tilde{X}^1A_1$, the $^3A_2$ and $^1A_2$ electronic states. The calculated value of the adiabatic excitation energy of the lower excited states has varied during the last decades [17,18]. But recent ab initio values [1a,2,5] for the transition to the $^3B_2$ state have been found to be close to experimental values. Specifically, Allan et al. [12] report a value of 1.297 eV (electron-energy loss spectroscopy). Arnold et al. [11] obtained a value of 1.30 eV from the dissociation of the O_3^- anion, and Anderson and co-workers [8,17–19] found 1.29 ± 0.03 eV by absorption spectroscopy. These values along with values for other states in this region are summarized in Table 1. In [8], the authors improved their results with a spectrometer able to detect ozone absorption features nine orders of magnitude weaker than the Hartley bands. They have successfully characterized the energy of the vibrational bands of the three lower triplet states ($^3A_2$, $^3B_2$, $^3B_1$) and determined their origin frequencies through a careful investigation from the near infrared to the visible absorption region using a combination of digital filtering and isotopic substitution.

In a more recent paper [20], these last authors also estimated the value of the asymmetric stretching frequency, ν_3, of the $^3A_2$ state to be 367 ± 17 cm^{-1} from the triplet state $^3A_2$ zero point energy. Recently, Xie et al. [21] determined accurate potential energy surface (PES) of the $^3A_2$ state from internally contracted multi-reference configuration interaction (icMRCI) based on the state-averaged complete active space self-consistent field (CASSCF) orbitals. The adiabatic and diabatic potential energies as well as the non-adiabatic coupling were computed. For the first time, the frequencies of all three vibrational modes were calculated theoretically. The antisymmetric stretching frequency is 422.2 cm^{-1} in the diabatic representation with the non-adiabatic coupling and 427.3 cm^{-1} from adiabatic PES without the non-adiabatic coupling. At the present time, experimental verification of this predicted band is lacking.

This paper is devoted to an analysis of the complex structure observed between 10,274 and 10,525 cm^{-1} that is superimposed on the 2_0^2 band of the Wulf transition, $^3A_2 \leftarrow \tilde{X}^1A_1$ (see Fig. 1a and b). Absorption spectra of both isotopomers, $^{16}O_3$ and $^{18}O_3$, have been studied. We have concluded that this spectral region is composed of two weak transitions. The first, located in blue, has a somewhat diffuse rotational sub-band structure while the other is completely diffuse and lacks any resolvable rotational structure.

The absorption features of the first transition are broadened by predissociation and are largely overlapped. This results in a spectrum characterized by broad undulations against the background continuum of the 2_0^2 $^3A_2 \leftarrow \tilde{X}^1A_1$ transition. Under these conditions, direct assignments are not possible. As a consequence, we have used the band contour method to confirm the nature of the transition and to determine approximate values of the main spectroscopic constants (rotational and spin–orbit constants). The geometry of the molecule of ozone in the upper vibrational level was determined from the observed constants. The band contour method also showed that the symmetry of this band is the same as that of the 0_0^0 and 2_0^1 bands of the $^3A_2 \leftarrow \tilde{X}^1A_1$ transition. We have justified the assignment of this cold band as 3_0^2 from both theoretical spectroscopic considerations and from a comparison between the spectra of the two isotopomers.

The other transition, in the red side of the region (Fig. 1a and b) and centered at 10,360 cm^{-1}, is structureless and weak. By comparison of the absorption spectra for the isotopomers $^{16}O_3$ and $^{18}O_3$, we propose its assignment as $^3B_2 \leftarrow \tilde{X}^1A_1$. This is in agreement with the recent works previously mentioned and presented in Table 1.

In the following sections, we describe the experiments used to obtain the absorption spectra at low temperatures, by Fourier transform spectroscopy (FTS) and intra cavity laser absorption spectroscopy (ICLAS). Section 3 contains a discussion of the modeling of the different possible transitions including a discussion of the symmetries of the wave-functions which compose the total wave-function for the singlet and the triplet states. Also included is a discussion of the coupling scheme, selection rules for the rotational quantum numbers and isotopic rules. In Section 4, the best calculated band contour obtained for the resolvable spectrum is presented along with the implications of its assignment as 3_0^2. To determine the nature of the diffuse unknown transition, we will discuss the different recent works in literature and select the best candidate based on observed isotopic shits and application of the isotopic rules.

is 10,469 ± 1 cm^{-1} (as can be seen in Fig. 2). Consequently, in Tables 2 and 4 of [16] T_0 of $^3B_2$ is 1.2966 ± 0.0006 eV or T_0 = 10,458 ± 5 cm^{-1} instead of 10,444 ± 5 cm^{-1}.

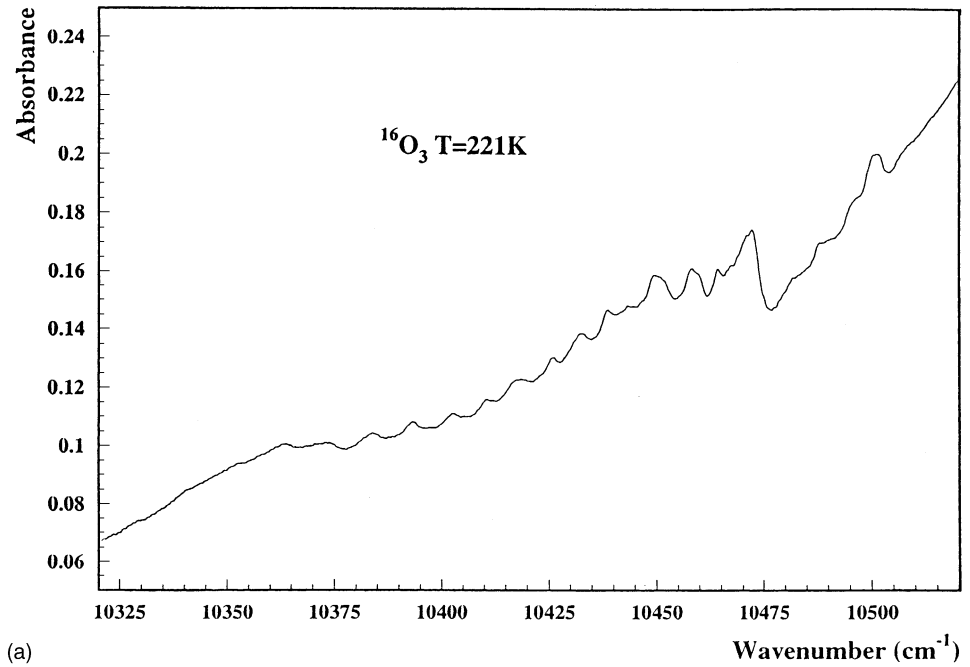

(a)

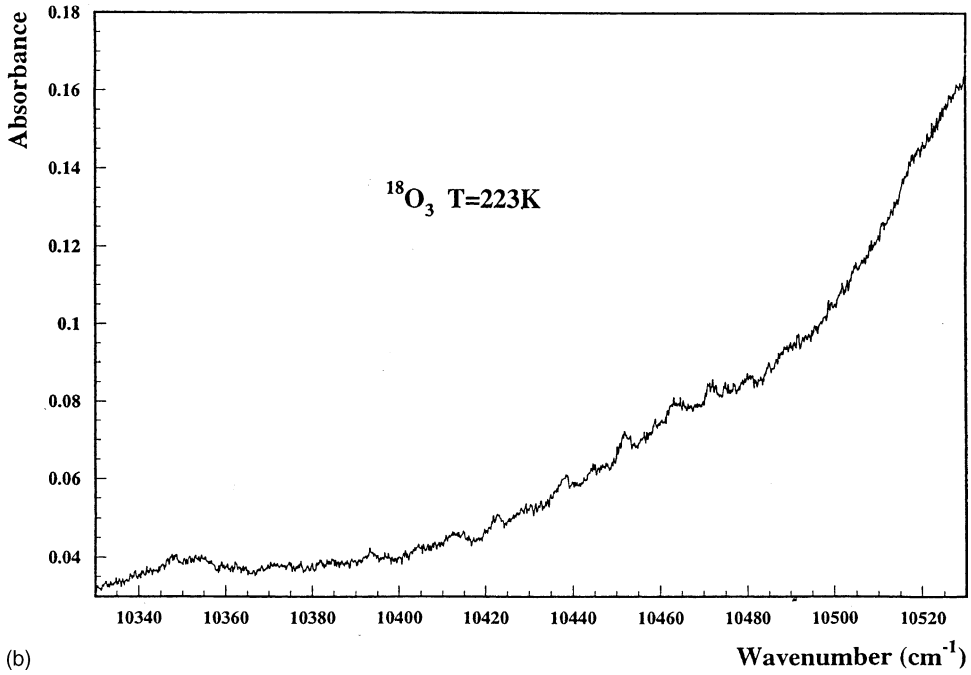

(b)

Fig. 1. (a) Absorption band of the $^3B_2 \leftarrow \tilde{X}^1A_1$ and $^3A_2(3_0^2) \leftarrow \tilde{X}^1A_1$ transitions for the isotopomer $^{16}O_3$ in the range 10,320–10,520 cm^{-1} obtained by Fourier transform spectrometry in our laboratory using the White cell of the Reims' laboratory [14a]. The resolution is 0.5 cm^{-1}, the optical path length (l) is 40 m, the ozone pressure is 110 Torr and the temperature is 221 K. (b) Absorption band of the $^3B_2 \leftarrow \tilde{X}^1A_1$ and $^3A_2(3_0^2) \leftarrow \tilde{X}^1A_1$ transitions for $^{18}O_3$ in the range 10,330–10,530 cm^{-1} obtained by FTS in our laboratory using the White cell of Reims. The resolution is 0.2 cm^{-1}, the optical path length is 80 m, the ozone pressure is 34.4 Torr and the temperature is 223 K.

2. Experiments

Earlier spectra were obtained with a White-type absorption cell set up in the "Laboratoire de Chimie-Physique" (Reims). The apparatus is described in our earlier papers [10a–c,14a–c,15]. This cell could be cooled to −50 °C and when coupled to a high resolution Fourier transform spectrometer, the absorption spectra for $^{16}O_3$ and $^{18}O_3$, shown in Fig. 1a and b, were obtained.

The principle of ICLAS is based on the fact that very weak absorption lines of an absorber molecule inside the cavity of a multi-mode laser can be observed superimposed on the broadband laser spectrum. ICLAS is a very sensitive and quantitative technique which provides equivalent path

lengths up a 100 km. It is therefore well suited for detecting low concentrations of absorbers or for systems with very low oscillator strengths. The experimental apparatus for ICLAS used here is based on a Ti-sapphire laser and has already been described in detail earlier [22–24].

The spectrum of the Ti-sapphire laser is time resolved and the duration, t_g, between the starting of the Ti-sapphire laser and the recording of the spectrum gives directly the equivalent path length $I_{eq} = (l/L)ct_g$, where l is the absorption path length, L the total optical length of the cavity, c the velocity of light and t_g the generation time. The spectra were recorded between 10,320 and 10,550 cm^{-1} with a generation time of the order of 100 μs. Taking into account, the 34% filling ratio of the laser cavity by the absorber, this corresponds to an equivalent absorption path length of 10.2 km. The spectrum is then dispersed by a high resolution spectrograph (resolution up to ≈800,000) and recorded by a 3752 photodiode array. The wavenumber calibration was achieved by using two reference lines due to atmospheric water vapour lines [25].

The spectral region investigated shows strong absorption by atmospheric water present in part of the laser cavity. In order to minimize the intracavity absorption of atmospheric water, a flow of dry nitrogen was permanently injected in the Ti-sapphire laser cavity leading to a decrease in water absorption, typically by a factor of 30. To further remove residual water absorption lines, we recorded one spectrum with an evacuated cavity cell containing traces of water vapour and one spectrum with a given pressure of ozone and the traces of water. Subtraction of the former from the latter provides the ozone absorption spectrum.

The spectrum located at the blue end of the region is mostly unresolved but does show some rotational structure. The absorption features have typical line widths of 5 cm^{-1} or more. Indeed, we could not further resolve the narrower absorption lines even by using our very high resolution spectrograph (resolving power of the order of 800,000). We then used a medium resolution spectrograph (Jobin-Yvon HRS 20, resolving power of the order of 10,000) to disperse the spectrum. This allowed us to record, as a whole, the total emission range of the Ti-sapphire laser which has a typical width of 60 cm^{-1} (full width at half maximum, FWHM). Since the absorption lines appear superimposed on the laser baseline, broad absorption features can hardly be extracted when their spectral widths are of the order of the laser spectral width itself. The procedure described above, using the subtraction of two spectra, was also adopted to reduce the baseline uncertainty of our ICLAS measurements.

The spectrum of ozone cooled to low temperature was obtained by using the intracavity cell previously designed for the ICLAS spectroscopy of the O_2 dimer [26]. It consists of three cylindrical stainless steel compartments. The inner-most cylinder (50 cm length, 2 cm diameter) contains the ozone sample and is fitted by two wedge shaped windows mounted at the Brewster angle. An MKS capacitance gauge is used to monitor the pressure. The inner compartment is surrounded by a cryogenic chamber containing liquid nitrogen (LN_2). The assembly is enclosed in a vacuum envelope fitted by two Brewster angle windows where a pressure of less than 10^{-4} Torr is maintained.

The cell was filled with ozone at a pressure of about 12 Torr at room temperature. The absorption signal at (LN_2) temperature is extremely weak as the ozone vapour pressure at 77 K is less than 0.1 Torr. Then the measurements were performed from the room temperature down to about 150 K by maintaining the level of LN_2 in the cryogenic chamber just below the inner tube containing ozone. The temperature, measured by a thermocouple sealed to the inner tube, was fixed by the thermal equilibrium between the inner tube and the gaseous nitrogen above LN_2. Fig. 2 shows the evolution of the absorption of ozone when the temperature decreases from 192 down to 161 K. A spectrum obtained with FTS at 220 K is added for comparison. If the FTS spectra are compared to the spectra obtained under the same conditions of pressure and temperature with ICLAS (Fig. 2 at 161 K), their quality are very similar. We will however prefer ICLAS spectra in this work for contour analysis because of its better resolution and signal-to-noise ratio. We will use the FTS spectra to measure absorbance and related cross-sections since the zero line is better defined in FTS than in ICLAS spectra.

A new variable temperature cell has been especially built in our group with the goal of using it to obtain accurate absolute absorption cross-sections. Our aim is to record spectra over a large range of wavelengths (from the near infrared to the UV region) and over large temperature ranges (from room temperature to 173 K). The latter temperature is of particular interest since it reproduces the lowest temperatures of the high polar atmosphere. A precise description of the cell design will be given in a forthcoming paper.

3. Theory

A forbidden singlet–triplet transition can become partially allowed by mixing some triplet character into the singlet state or some singlet character into the triplet state. The $\tilde{X}^1A_1$ ground state of ozone is energetically well separated from the $^3B_2$ or $^3B_1$ triplets which are still higher than $^3A_2$ previously identified [10,14]. So it is probably a mixing of the triplet states with another singlet electronic state which induces an intensity transfer to the singlet–triplet forbidden transition. Indeed, it was suggested that the $^3A_2$ state could gain intensity through spin–orbit mixing with the $^1B_2$ state [27] (responsible for the strong UV Hartley bands). Later the singlet–triplet absorption properties of $^3A_2$ calculated from spin–orbit configuration interaction [28] or from multi-configuration quadratic response function [29] gave an estimate of the role of $^3A_2$ in the Wulf bands.

The $\tilde{X}^1A_1$ ground state rovibrational energies are well known and have been determined with high precision. Our analysis will use either the term values determined by Flaud

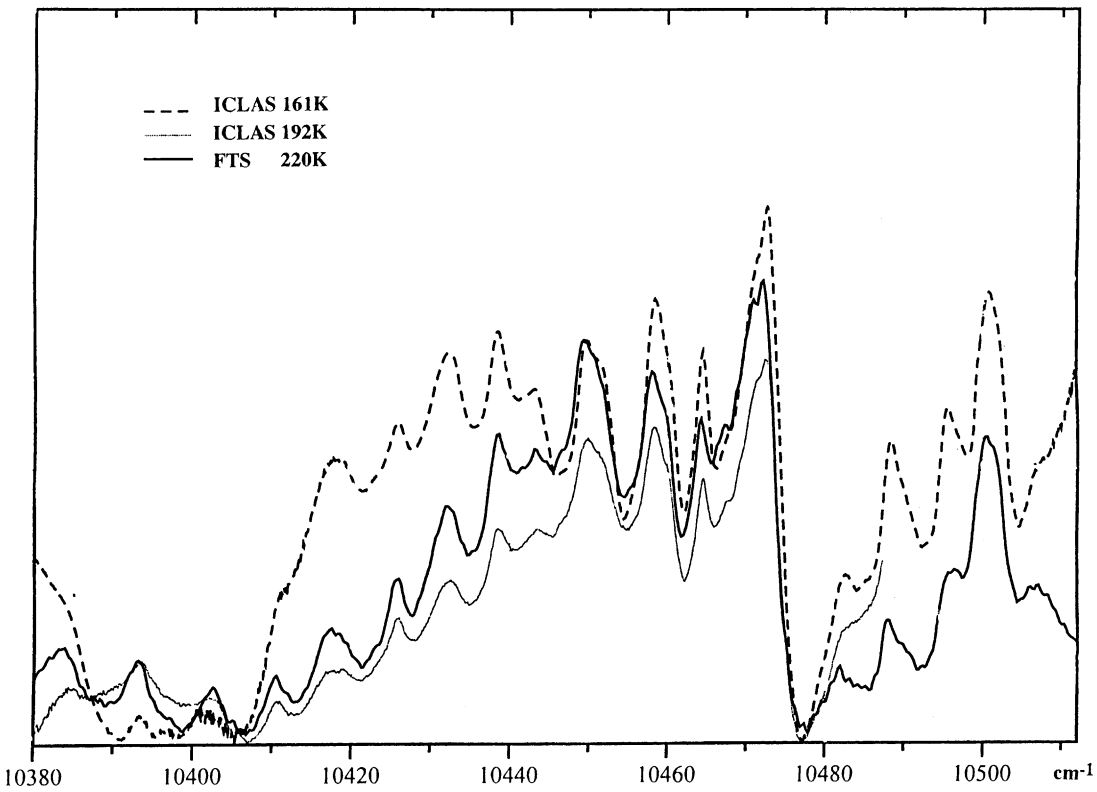

Fig. 2. Comparison of absorption spectra obtained by ICLAS and FTS: ICLAS in Grenoble for two temperatures 192 K (4.95 Torr) and 161 K (5.2 Torr) (the dashed line and the thin line, respectively) and FTS in Villeurbanne with the White cell of Reims (thick line) at 220 K (the lowest temperature given by the cell) [14a]. For this last spectrum, the continuous background of the $^3A_2(1_0^0 2_0^2 3_0^0)$ band has been suppressed by computer aided subtraction. As the zero level of absorbance cannot be determined in the case of ICLAS, the absorbance scale is not significant in this figure.

[30a] from infrared rotation–vibration spectra or, the polynomial development established from several microwave and infrared studies of the ground state [31–33]. The Hamiltonian is that given by Watson [34] with quartic and sextic distortion coefficients as described by Flaud et al. [35]. These latter authors recalculate the positions of the lines for the first rotation–vibration bands in the ground state with a root-mean-square deviation (RMS) of the order of $3 \times 10^{-4}\,cm^{-1}$.

As previously described [10,14–16], $^{16}O_3$ and $^{18}O_3$ belong to the C_{2v} point group if the asymmetric deformations from the equilibrium geometry are neglected. Triplet states ($^3B_2$ or $^3B_1$) in the same energy region as $^3A_2$, will likely obey Hund's case (b) coupling. Molecules for which the case (b) Hamiltonian has been successfully used include H_2CO [36], SO_2 [37,38] and recently $^{16}O_3$ ($^3A_2$) [10,14–16]. In this situation, the spin splittings of the triplet state in the non-rotating molecule are small relative to the rotational intervals. Under this coupling scheme, the spin angular momentum, S, and the angular momentum for molecular rotation, N, couple to form a resultant J, the total angular momentum of the molecule (excluding nuclear spin). The rotational levels are then labeled by the quantum numbers J, N, K_a and K_c. For a fixed value of N, three spin components exist: $F_1(J = N + 1)$, $F_2(J = N)$ and $F_3(J = N - 1)$. The F_i values are not good quantum numbers and they do not refer to state labels since the three spin states are completely mixed by rotation in the case (b) limit.

A I^r representation ($a \Leftrightarrow z$, $b \Leftrightarrow x$, $c \Leftrightarrow y$) is adopted in correlating the inertial axes with the symmetry axes. It supposes that the inertial x axis coincides with the C_2 axis of symmetry. In standard point group axis conventions, this symmetry axis is labeled z and to avoid confusion, translational and rotational vectors in this paper will be noted as T_{abc} and R_{abc} [14a]. As a consequence, the usual rotational constants for the nearly symmetric top prolate molecule are $A(z) > B(x) > C(y)$. We have followed the same character table and nomenclature as that used by Brand et al. [37] in their analysis of SO_2. Specifically, the species of a vector perpendicular to the molecular plane remains as b_1. Thus the vibrational modes of ozone (ν_1 symmetric stretch, ν_2 bending mode, and ν_3 antisymmetric stretch) have the usual symmetries A_1, A_1, and B_2, respectively. The three spin functions transforming as A_2 (R_b), B_2 (R_c) and B_1 (R_a). The dipole moment operator about the molecule fixed axis is μ_g ($g = a$, b, or c with symmetry B_2, A_1, B_1, respectively). The species of the dipole moment operator also determines the symmetry species of the singlet state from which intensity borrowing occurs.

All vibronic bands in our earlier analysis of this spectral region involve either ν_1 or ν_2 and belong to the same electronic transition, $^3A_2 \leftarrow \tilde{X}^1A_1$. The bands have a similar

rotational band profile and follow $\Delta K_a = 0, \pm 2$ and $\Delta K_c = 0, \pm 2$ selection rules. The new band centered at 10,500 cm^{-1} is assigned to the same $^3A_2 \leftarrow \tilde{X}^1A_1$ electronic transition but involves excitation of two quanta of ν_3 (3_0^2 vibronic transition). A spectroscopic argument can be made to show that only cold bands with even quanta of ν_3 will have significant intensity. Singlet–triplet transitions are similar to electronically allowed singlet–singlet transitions in the selection rules on vibrational transitions within the electronic transition. This follows since the vibrational overlap integral, $\langle v''|v' \rangle$, can be factored out of the total wave-function in both cases. In an electronically allowed singlet–singlet transition or singlet–triplet transition made allowed by spin–orbit interactions, the vibrational integral $\langle v''|v' \rangle$ must be totally symmetric (A or A_1). For cold bands this means only symmetric transitions or even quanta of asymmetric vibrations are allowed. The only way we will see odd quanta of ν_3 in cold band structure will be through a vibronic spin–orbit mechanism. Calculations performed for selenoformaldehyde [39] show that this mechanism is considerably less efficient, about 100 times weaker. The symmetry of this transition is identical to the well-known symmetry of the 0_0^0 and 2_0^1 bands of $^3A_2 \leftarrow \tilde{X}^1A_1$ and selection rules are: $\Delta J = 0, \pm 1$, $\Delta N = 0, \pm 1, \pm 2$, $\Delta K_a = 0, \pm 2$, and $\Delta K_c = 0, \pm 2$.

The other transition in this region is structureless, very weak and centered at 10,363 cm^{-1} for $^{16}O_3$. It probably belongs to $^3B_2 \leftarrow \tilde{X}^1A_1$. Following our conventions presented at the beginning of Section 3 of this work and in our paper [14a], we can establish the correspondence between symmetries with C_{2v} and D_{2h} geometry: B_2 corresponds to B_{1u} and B_1 to B_{2u}, respectively (Table 4 in [40]). So, transitions to the $^3B_2$ and $^3B_1$ states follow the symmetry rules: for transitions to the $^3B_2$ state, $\Delta J = 0, \pm 1$, $\Delta N = 0, \pm 1, \pm 2$, $\Delta K_a = 0, \pm 2$, and $\Delta K_c = \pm 1, \pm 3$ and for the $^3B_1 \leftarrow \tilde{X}^1A_1$ transition, $\Delta J = 0, \pm 1$, $\Delta N = 0, \pm 1, \pm 2$, $\Delta K_a = \pm 1, \pm 3$ and $\Delta K_c = \pm 0, \pm 2$.

The program developed by Judge et al. [40,41], using the Hamiltonian of Raynes [42] and intensities determined by Creutzberg and Hougen [43,44], simulates singlet–triplet absorption spectra. A comparison of the experimental and calculated band contour allow one to determine approximate values of the spectroscopic constants. Because of the quality of the spectra, we have limited the determination to a selected set of constants: *A*, *B*, *C* constrained somewhat to the geometry given by the theoreticians [1,2] and the spin–spin constants α and β. The other, relatively small constants (such as the distortion constants $d_k, d_{jk}, d_j, \ldots$, etc. and the spin–rotation constants a_0, *a* and *b*), were constrained in the various simulations to the corresponding values of the $^3A_2$ state [14a–c].

4. Results and discussion

The FTS absorption spectra of the two isotopomers $^{16}O_3$ and $^{18}O_3$ are shown in Fig. 3a and b, respectively. They are obtained after removal of the $^3A_2 \leftarrow \tilde{X}^1A_1$ continuous background of the 2_0^1 band. Since the absorption spectra of $^{18}O_3$ is noisy, we have limited our study to $^{16}O_3$ and have used the ICLAS spectra at 161 K in the fitting procedure. This spectrum is well extended to the blue side of the region and the resolution of the rotational structure is better than that obtained with FTS.

Two distinct absorption profiles, probably corresponding to two different electronic transitions, can be distinguished in the region from 10,300 to 10,525 cm^{-1} for both isotopomers. This conclusion is supported by our simulations. The simulated spectra for the 10,400–10,525 cm^{-1} region never extend into the 10,300–10,380 cm^{-1} region at low temperatures.

Initially, we had thought that the band, located in the 10,400–10,525 cm^{-1} region, involved a transition to the $^3B_2$ state. The band contour simulation gave a reasonably acceptable fit to the experiment. But in order to reproduce the double hump of the spectrum, we were obliged to hugely change the two spin–spin constants (−5.0 and −9.1) instead of −0.56 and −0.8 as previously obtained for $^3A_2$ (0_0^0) [14a]. Such a large change in the spin constants is unlikely but possible since the interaction of the spin components of the $^3B_2$ state with other excited states would be different than that of the $^3A_2$ state. But given the arguments presented in earlier sections of this paper and the low predicted oscillator strength of transitions to this state [45,46], the transition in this region is thought to be to the $2\nu_3$ state of $^3A_2 \leftarrow \tilde{X}^1A_1$. With the ab initio geometry of ozone [1a–c,2] as a guide, we have varied the values of the rotational constants *A*, *B*, and *C* in order to get good agreement with the experimental band contour. The fitting procedure was constrained by two factors. Firstly, we required that the vertex angle calculated from the trial rotational constants be close to the theoretically predicted value. Secondly, the different distortion constants, the spin–rotation constants (a_0, *a* and *b*) and the α, β spin–spin constants, be fixed at the values previously determined for the $^3A_2$ state [14a–c]. Our best simulation for $^{16}O_3$ (Fig. 4) is obtained with 102° and $r_e = 1.36$ Å. This was obtained with $A = 2.158\ cm^{-1}$, $B = 0.472\ cm^{-1}$ and $C = 0.387\ cm^{-1}$.

An important requirement in the fitting of spectra by the band contour method is the correct choice of the mean value for the FWHM of the rotational lines. Two previous papers showed the wide variation of the broadening of the lines with *J* and *K* within the various F_i components [14c,15]. It is obvious that a mean value for the FWHM can only be a rough approximation. We found previously that a FWHM of about 0.4 cm^{-1} gave a satisfactory contour for the 2_0^1 band of $^3A_2 \leftarrow \tilde{X}^1A_1$ transition [14c]. However, for the transition in the 10,500 cm^{-1} region, the predissociation broadening seems to be stronger and the theoretical contour obtained with a FWHM = 2.2 cm^{-1} gave the best fit. In our simulation, we have limited the maximum value of *J* at 20 and K_a to 4. This is in

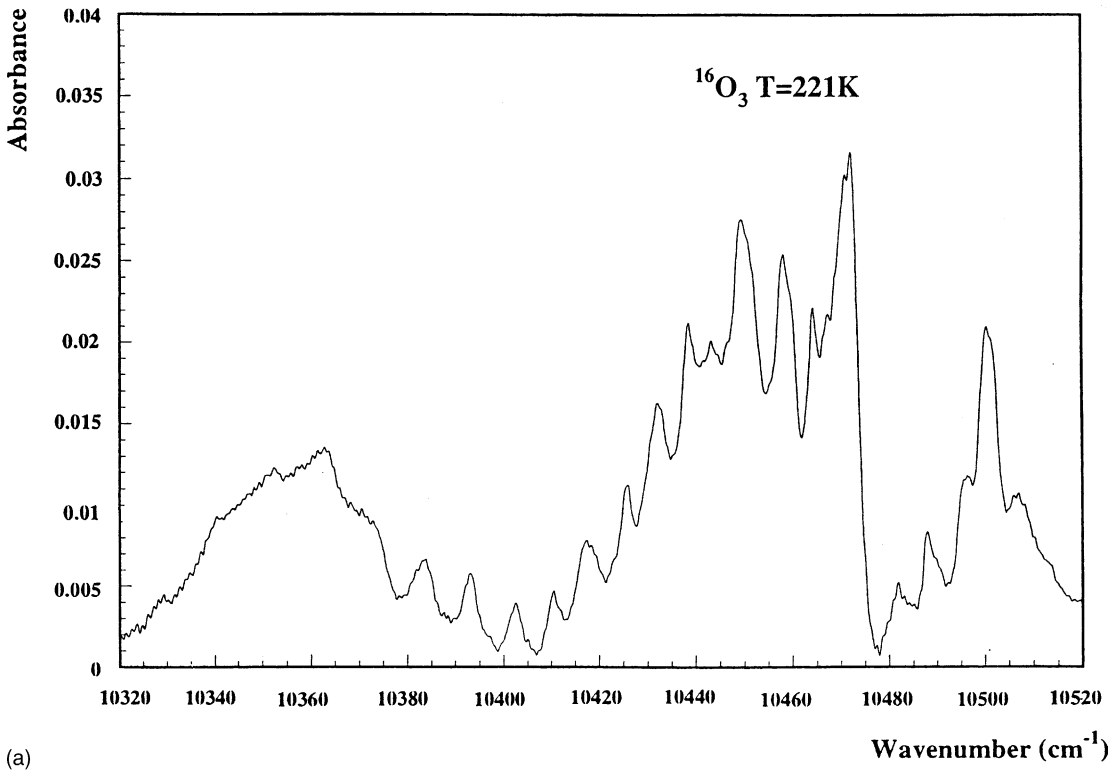

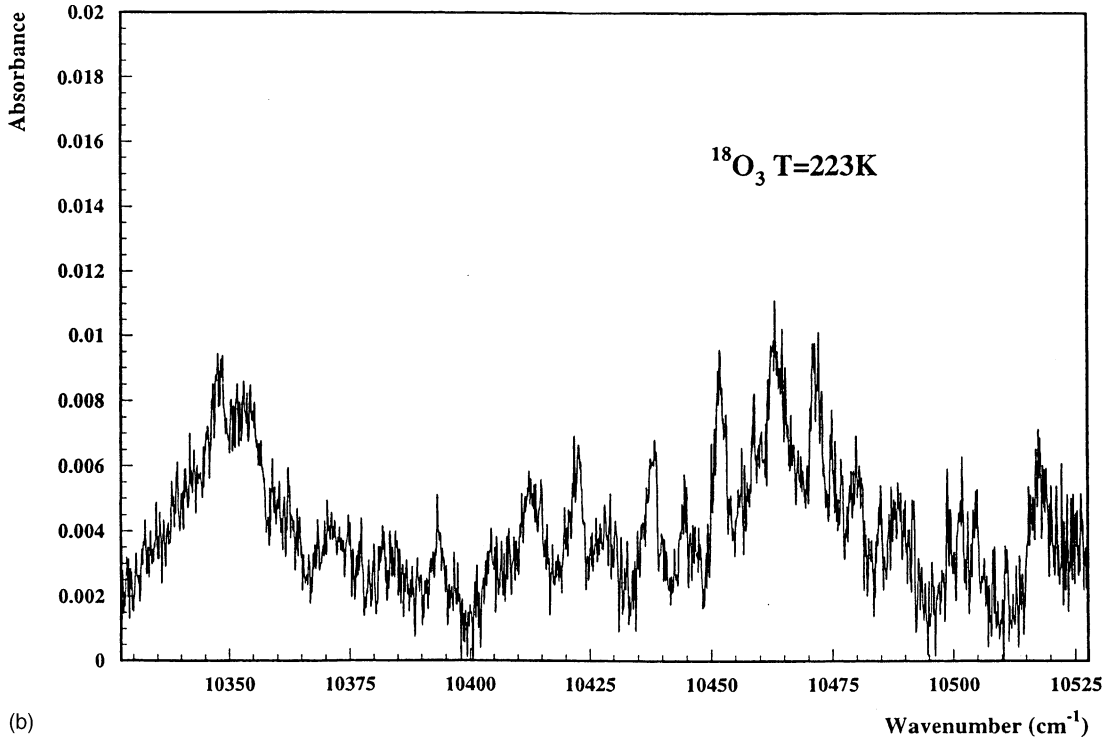

Fig. 3. (a) Absorption spectrum of ozone $^{16}O_3$ of the Fig. 1a after removal of the background. (b) Absorption spectrum of ozone $^{18}O_3$ of the Fig. 1b after removal of the background.

agreement with our experimental condition of temperature ($T = 161$ K).

The results of our analysis of this region can be summarized as follows.

4.1. $^3A_2 \leftarrow \tilde{X}^1A_1$ system

The origins of the transitions for both $^{16}O_3$ and $^{18}O_3$ were determined by the band contour method to be at $10{,}473 \pm 3$

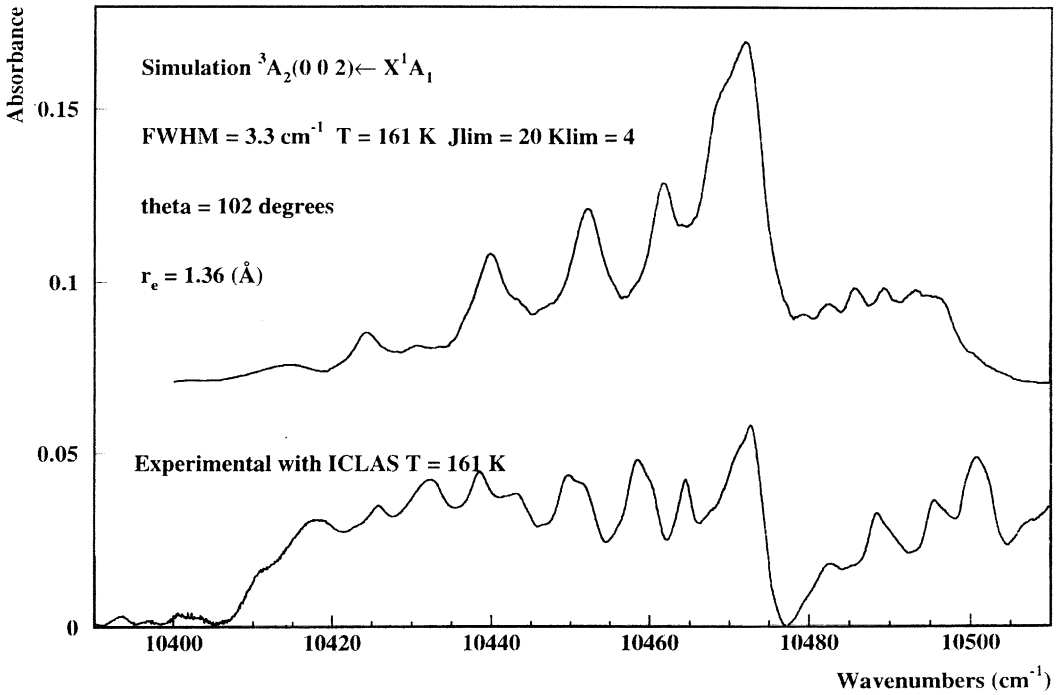

Fig. 4. Simulation of a rovibrational band of the electronic transition: $^3A_2(3_0^2) \leftarrow \tilde{X}^1A_1$ compared to the experimental spectrum obtained by ICLAS technique at 161 K. The theoretical contour is calculated with $\theta = 102^\circ$ the mean value of the top angle calculated recently [1a–c,2]. The full width at half maximum is 2.2 cm^{-1}, the maximum value of J is $J_{\text{lim}} = 20$ and $K_{\text{lim}} = 4$ for the maximum value of K. The spectroscopic constants relative to the excited state $^3A_2$ are given in [14a]. We choose for the two active components μ_x and μ_y of the dipole transition moment, the relative value $\mu_x/\mu_y = 100$. The rovibrational energies of the ground state $\tilde{X}^1A_1$ (0 0 0) are calculated from the spectroscopic constants of De Backer [33].

and 10,462 ± 3 cm^{-1}, respectively, and are close to the maximum intensity of the band profile. These values, when subtracted from the origin of the 0_0^0 band of this system [14a–c] give directly $(2\nu_3)_{16} = 920\,\text{cm}^{-1}$ and $(2\nu_3)_{18} = 888\,\text{cm}^{-1}$. If anharmonicity in this mode is ignored, then $(\nu_3)_{16} = 460 \pm 2\,\text{cm}^{-1}$. This value is larger than that inferred by Anderson and Mauersberger [8] ($\nu_3 = 367 \pm 17\,\text{cm}^{-1}$) as determined from the zero-point energy. Our estimate of 460 cm^{-1} can be misleading since, as noted in [21], the potentials for the $^3A_2$ state are anharmonic. This is particularly true for the antisymmetric stretching mode in this state. Nevertheless, our value is comparable to that calculated by Xie et al. (422.2 (427.3) cm^{-1}) [21] from their accurate PES, which gave values of ν_2 and ν_1 frequencies close to those obtained in [20] (see Table 2 in [21]). The question does remain, however, about the magnitude of the anharmonicity. An estimate of the range can be given. If we transfer the effective anharmonicity obtained from the ν_2 mode of $^3A_2$ (0, 2, 0) = 1002.5 (1010.3) cm^{-1} in Table 2 of [21], this would give $^3A_2$ (0, 0, 1) a lower range of 455.7 (456.7) cm^{-1} and if we use the ν_3 mode in the ground state of $^{16}O_3$: (0, 0, 2) = 2057.891 cm^{-1} (Table 5 of [30b]), this would give an upper range of 465.9 cm^{-1}. From our two frequencies, the observed isotopic ratio $[(\nu_3)_{18}/(\nu_3)_{16}]_{\text{exp}}$ is 0.966 with $(\nu_3)_{18} = 444\,\text{cm}^{-1}$. This is comparable to the theoretical value of 0.943 predicted from the isotopic rule. The heavier isotopomer is red-shifted (as expected) from the lighter by 11 cm^{-1}. This is quite similar to the red-shift observed for the $^3A_2(2_0^1) \leftarrow \tilde{X}^1A_1(0_0^0)$ band system (5 cm^{-1} [8] or (−7.06 cm^{-1}) [14c]).

4.2. $^3B_2 \leftarrow \tilde{X}^1A_1$ system

The lower energy part of the observed region is quasi-continuous and forms a hump that does not show rotational fine structure even at our lowest temperatures. This hump is centered at about 10,363 cm^{-1} for $^{16}O_3$ and 10,354 cm^{-1} for $^{18}O_3$. It is difficult to measure the isotopic shifts in the case of diffuse bands, since the band maxima will not necessarily correspond to the same quantum numbers for both isotopomers. Consequently, the observed frequency shift calculated from this method will be the sum of various effects (contour shift and isotopic shifts). However, we think that an error of 5–10 cm^{-1} is reasonable. With these remarks, we can infer that the centers of the diffuse bands are the origins of the transition and that they are red-shifted by $9 \pm 3\,\text{cm}^{-1}$ ($\nu(^{18}O_3) - \nu(^{16}O_3)$). The origin band of this new system should be blue-shifted, probably by a comparable amount as seen for the $^3A_2 \leftarrow \tilde{X}^1A_1$ band system (+20 cm^{-1}). Consequently, these new bands are probably not origin bands, but may be a transition with one quantum of an excited state vibration. Two likely assignments are possible.

(i) If it is the 2_0^1 band and if the bending mode frequency is approximately that of the $^3A_2$ state, i.e. 550 cm^{-1},

then the origin band of the new system would be at about 9810 cm^{-1}. The origin band of this new system would then overlap the red end of the 2_0^1 band of $^3A_2 \leftarrow \tilde{X}^1A_1$. However, this band is likely to be weak based on Franck–Condon arguments and the band which is diffuse anyway, would disappear under the very intense 2_0^1 band of the $^3A_2 \leftarrow \tilde{X}^1A_1$ transition. We recall that in the case of $^{18}O_3$, the 2_0^1 band of $^3A_2$ is particularly difficult to analyze because it is quite diffuse and only a few rotational lines were assigned.

(ii) If it is the 1_0^1 band (i.e. with a symmetric stretch quantum at about 1100 cm^{-1}) the origin band for the new system would be located at 9263 cm^{-1}. However, we see no O_3 absorption in this area.

There is still a lingering doubt about the correct assignment of the upper electronic state for this transition: is it $^3B_2$ or $^3B_1$? We suggest that it is probably $^3B_2$. Experiments of Arnold et al. [11] locate the $^3B_2$ state 10,449 cm^{-1} above the ground state and Günther and Anderson [20] have also assigned absorption in this region to the $^3B_2 \leftarrow \tilde{X}^1A_1$ transition. Recent studies place the $^3B_1$ state higher in energy than the $^3B_2$ state. Anderson and Arnold (experiment), Borowski et al. [1] and Banichevich and others [5,6] (theory) place the $^3B_1$ state about 11,700 cm^{-1} above the ground state (see Table 1), while Tsuneda et al. [2] locates it in the same region as $^3B_2$. The recent paper by Xie et al. [21], by citing Braunstein et al. [28] and, Minaev and Agren [29], suggests that the transition to $^3B_2$ will not be observable since its oscillator strength is much weaker than transitions to either the $^3A_2$ or $^3B_1$ states by a factor of nearly 100. Our measurements show that, although the band is quite weak, it is observable. We found that the maximum cross-section (α_{max}) at 139 K for the transition to this band is about 50 times weaker than the σ for the corresponding transition to the 2_0^1 band of the $^3A_2$ state. If we assume that the ratio of the σ values for individual bands accurately reflects the ratio of the oscillator strengths for the two electronic transitions, then the experimental value is quite close to that predicted from theory.

5. Conclusion

This work shows the difficulty in attempting to fit the rotationally diffuse 3_0^2 band of the Wulf transition, recorded in the region 10,274–10,525 cm^{-1}. The situation is substantially worse than in the case of the 2_0^1 band of the $^3A_2 \leftarrow \tilde{X}^1A_1$ transition [14c] for which a partial rotational analysis was possible. The dissociation processes seen in the 3_0^2 band are so strong that they greatly wash out the rotational fine structure except for some low K_a, $\Delta K_a = 0$, ± 2 sub-bands. Similar to the case of the $^3A_2$ state, the origin of the $^3B_2$ state is located in a region of high bound or quasi-bound rovibrational levels of the ground $\tilde{X}$ state (v about 10 [45]). These levels are probably more and more dense with increasing energy and so it is not surprising that the spectra appear more and more diffuse.

In spite of the diffuse nature of the spectra, some conclusions are however possible from the present work. Thanks to a comparison of $^{16}O_3$ and $^{18}O_3$ spectra, we can estimate, for the first time, an observed experimental value for the ν_3 mode of the $^3A_2$ state at 460 ± 2 cm^{-1}. This value is close to the previous result of 367 cm^{-1} [20] calculated from combining experimental data with the adiabatic energy. It is quite close to a recent theoretical calculation [21] of 422 cm^{-1}. The band contour method was used to determine a set of rotational constants. However, the method gave only rough agreement between the calculated and observed spectra.

We also give an approximate value for the origin of the $^3B_2 \leftarrow \tilde{X}^1A_1$ transition and we suggest that the observed band is probably excited by one quantum of the symmetric bend.

We have demonstrated here that the moderately low temperature, high resolution ICLAS technique (like the high resolution FTS technique) does not produce spectra with resolvable, assignable rotational features (see Fig. 4). In the future, we plan to improve our absorption spectra. A supersonic jet of ozone observed with ICLAS [22] or CW-CRDS (cavity ring-down spectroscopy) [46] techniques is probably the best way to obtain measurable absorption with high resolution at very low temperatures. The new experiments will lead to considerably simplified absorption spectra, with comparatively few lines that correspond to the low values of the rotational quantum numbers J and K (rovibrational levels of $\tilde{X}^1A_1$ populated at Boltzmann equilibrium). If, among these lines, some are not predissociated or only weakly predissociated, a full line-by-line least-squares analysis would be possible. Such an analysis would confirm the nature of the $^3B_2$ electronic upper state implied in this study.

Acknowledgements

We greatly acknowledge J.M. Flaud for transferring to us the term values of infrared rotation–vibration spectra. R.H.J. wishes to gratefully acknowledge the support of the National Science Foundation (USA) and the donors to the Petroleum Research Fund, administered by the American Chemical Society, for support of this work.

References

[1] (a) P. Borowski, M. Fülcher, P.-A. Malmqvist, B.O. Roos, Chem. Phys. Lett. 237 (1995) 195;
(b) P. Borowski, K. Andersson, P.-A. Malmquist, B.O. Roos, J. Chem. Phys. 97 (1992) 5568.
[2] T. Tsuneda, H. Nakano, K. Hirao, J. Chem. Phys. 103 (1995) 6520.
[3] M. Braunstein, P.J. Hay, R.L. Martin, R.T. Pack, J. Chem. Phys. 95 (1991) 8239.
[4] M. Braunstein, R.T. Pack, J. Chem. Phys. 96 (1992) 6378–6388.
[5] A. Banichevich, S.D. Peyerimhoff, Chem. Phys. 174 (1993) 93.

[6] A. Banichevich, S.D. Peyerimhoff, F. Grein, Chem. Phys. 178 (1993) 155.
[7] P.G. Szalay, R.J. Bartlett, J. Chem. Phys. 101 (1994) 4936.
[8] S.M. Anderson, K. Mauersberger, J. Geophys. Res. 100 (1995) 3033.
[9] S.M. Anderson, K. Mauersberger, J. Morton, The ozone molecule: isotope effects and electronic structure in current problems and progress in atmospheric chemistry, in: J.R. Barker (Ed.), Advanced Series in Physical Chemistry, vol. 3, World Scientific Publishing, Singapore, 1995.
[10] (a) A.J. Bouvier, B. Bussery, S. Churassy, D. Inard, M. Nota, V. Veyret, R. Bacis, F. Bohr, J. Brion, J. Malicet, in: Proceedings of the Third European Symposium on Polar Stratospheric Ozone Research, vol. 707, Schliersee, Bavaria FRG, 1996;
(b) A.J. Bouvier, R. Bacis, B. Bussery, S. Churassy, D. Inard, M. Nota, J. Brion, J. Malicet, S.M. Anderson, Chem. Phys. Lett. 255 (1996) 263;
(c) D. Inard, Ph.D. thesis, Caracterisation spectroscopique d'un état métastable de l'ozone, Université Lyon I, France, second part, June 1997, 320 pp.
[11] D.W. Arnold, C. Xu, E.H. Kim, D.M. Neumark, J. Chem. Phys. 101 (1994) 912.
[12] M. Allan, N.J. Mason, J.A. Davies, J. Chem. Phys. 105 (1996) 5665.
[13] W.M. Johnstone, N.J. Mason, W.R. Newel, P. Biggs, G. Marston, R.P. Wayne, J. Phys. B 25 (1992) 3873.
[14] (a) A.J. Bouvier, D. Inard, V. Veyret, B. Bussery, R. Bacis, S. Churassy, J. Brion, J. Malicet, R.H. Judge, J. Mol. Spectrosc. 190 (1998) 189;
(b) A.J. Bouvier, V. Veyret, I. Russier, D. Inard, S. Churassy, R. Bacis, J. Brion, J. Malicet, R.H. Judge, Spectrochim. Acta A 55 (1999) 2811;
(c) A.J. Bouvier, G. Wannous, S. Churassy, R. Bacis, J. Brion, J. Malicet, R.H. Judge, Spectrochim. Acta A 57 (2001) 561.
[15] D. Inard, A.J. Bouvier, R. Bacis, S. Churassy, F. Bohr, J. Brion, J. Malicet, M. Jacon, Chem. Phys. Lett. 287 (1998) 515.
[16] R. Bacis, A.J. Bouvier, J.M. Flaud, Spectrochim. Acta A 54 (1998) 17.
[17] S.M. Anderson, J. Morton, K. Mauersberger, J. Chem. Phys. 93 (1990) 3826.
[18] S.M. Anderson, J. Maeder, K. Mauersberger, J. Chem. Phys. 94 (1991) 6351.
[19] S.M. Anderson, P. Hupalo, K. Mauersberger, J. Chem. Phys. 99 (1993) 737.
[20] S. Günther, S.M. Anderson, G. Hilpert, K. Mauersberger, J. Chem. Phys. 108 (1998) 5449.
[21] D. Xie, H. Guo, K.A. Peterson, J. Chem. Phys. 115 (2001) 10404.
[22] A. Campargue, F. Stoeckel, M. Chenevier, Spectrochim. Acta Rev. 13 (1990) 69.
[23] A. Kachanov, A. Charvat, F. Stoeckel, J. Opt. Soc. Am. B 11 (1994) 2412.
[24] M. Herman, J. Lievin, J. Vander Auwera, A. Campargue, Adv. Chem. Phys. 108 (1999) 1.
[25] L.S. Rothman, C.P. Rinsland, A. Goldman, S.T. Massie, D.E. Edwards, J.M. Flaud, A. Perrin, C. Camy-Perret, V. Dana, J.Y. Mandin, J. Schroeder, A. Mc Cann, R.R. Gamache, R.B. Wattson, K. Yoshino, K.V. Chance, K.W. Jucks, L.R. Brown, V. Nemtchinov, P. Varanasi, J. Quant. Spectrosc. Radiat. Transfer 60 (1998) 665.
[26] A. Campargue, L. Biennier, A. Kachanov, R. Jost, B. Bussery-Honvault, V. Veyret, S. Churassy, R. Bacis, Chem. Phys. Lett. 289 (1998) 734.
[27] M. Braunstein, R.T. Pack, J. Chem. Phys. 96 (1992) 6378.
[28] M. Braunstein, R.L. Martin, P.J. Hay, J. Chem. Phys. 102 (1995) 3662.
[29] B. Minaev, H. Agren, Chem. Phys. Lett. 217 (1994) 531.
[30] (a) J.M. Flaud, private communication;
(b) J.M. Flaud, R. Bacis, Spectrochim. Acta A 54 (1998) 3.
[31] J.M. Flaud, C. Camy-Peyret, V. Malathy Devi, C.P. Rinsland, M.A.H. Smith, J. Mol. Spectrosc. 124 (1987) 209–217.
[32] A. Barbe, C. Secroun, P. Jouve, N. Monnanteuji, J.C. Depannemaecker, B. Duterage, J.B. Bellet, P. Pinson, J. Mol. Spectrosc. 64 (1977) 343–364.
[33] M.R. De Backer, Thesis Reims, 1995.
[34] J.K. Watson, J. Chem. Phys. 46 (1967) 1935–1949.
[35] J.M. Flaud, C. Camy-Peyret, A. Barbe, S.C. Secroun, P. Jouve, J. Mol. Spectrosc. 80 (1980) 185–199.
[36] D.J. Clouthier, D.A. Ramsay, Annu. Rev. Phys. Chem. 34 (1983) 31, and references therein.
[37] J.C.D. Brand, V.T. Jones, C. Di Lauro, J. Mol. Spectrosc. 40 (1971) 616–631.
[38] K.E. Hallin, Y. Hamada, A.J. Merer, Can. J. Phys. 54 (1976) 2118–2127.
[39] D.C. Moule, L. Chantranupong, R.H. Judge, D.J. Clouthier, Can. J. Chem. 71 (1993) 1706–1712.
[40] R.H. Judge, A.A. Korale, J.J. York, D.L. Joo, D.J. Clouthier, D.C. Moule, J. Chem. Phys. 103 (1995) 5343.
[41] R.H. Judge, A.A. Korale, J.J. York, D.L. Joo, D.J. Clouthier, D.C. Moule, Comp. Phys. Commun. 93 (1996) 241.
[42] W.T. Raynes, J. Chem. Phys. 41 (1964) 3020.
[43] F. Creutzberg, J.T. Hougen, Can. J. Phys. 45 (1967) 1363.
[44] F. Creutzberg, J.T. Hougen, J. Mol. Spectrosc. 38 (1971) 257.
[45] F. Perez-Bernal, J.M. Arias, A. Frank, R. Lemus, R. Bijker, J. Mol. Spectrosc. 184 (1997) 1.
[46] D. Romanini, A.A. Kachanoy, N. Sadeghi, F. Stoeckel, Chem. Phys. Lett. 264 (1997) 316.